Development and characterisation of perforated release film interleaves for precise mode II fracture toughness control in high-performance composites

Czél G.

Composites: Part A 207 (2026) 109743

Contents lists available at ScienceDirect

Composites Part A

journal homepage: www.elsevier.com/locate/compositesa

Development and characterisation of perforated release film interleaves for precise mode II fracture toughness control in high-performance composites

Gergely Czél

Department of Polymer Engineering, Faculty of Mechanical Engineering, Budapest University of Technology and Economics, Műegyetem rkp. 3, H-1111 Budapest, Hungary
MTA-BME Lendület Sustainable Polymers Research Group, Budapest University of Technology and Economics, Műegyetem rkp. 3, H-1111 Budapest, Hungary

ARTICLE INFO

Keywords:
Interleaving
Glass fibre
Epoxy
Fracture toughness
Mechanical testing
Intermittent interlaminar bonding
Laser-cut

ABSTRACT

Perforation patterns with different interlaminar contact area ratios (ICARs) were designed for a 15 μm thick ethylene tetrafluoroethylene (ETFE) release film to modify the interface of unidirectional (UD) glass fibre/epoxy composite plates. The adhesion between the layers was reduced by partially separating the ply blocks with the release film, allowing only the epoxy to connect the layers through the circular perforations with diameters of 1 mm and 1.5 mm. After laser cutting, the resulting perforation pattern geometries were compared with the nominal ones using an image dimension measurement system. Cut central layer, UD prismatic coupons were tested under uniaxial tension to assess the mode II fracture toughness (G_{IIC}) of the laminates. A strong linear trend with increasing ICAR was observed, enabling precise control of the composite layer interface G_{IIC} through interleaf perforation pattern design.

1. Introduction

Fibre-reinforced composites are an excellent choice for weight-critical structural applications, allowing stiffness and strength to be tailored to match the loads expected during operation. However, their inhomogeneous and anisotropic microstructure, along with their poor out-of-plane tensile and interlaminar shear strength (due to their layered structure), pose major challenges for design engineers. Mode I and II fracture toughness (G_{IC} and G_{IIC}, respectively) of composite layer interfaces are also key design allowables that have long been investigated, and significant effort has been devoted to increasing them. Modification of the matrix material of the composite is proven to be one of the most straightforward approaches. Rubber particles, as well as nano-scale additives (e.g., carbon nanotubes, graphene), have been widely investigated and found to be effective in toughening composite laminates [1–4]. A unique opportunity to enhance interlaminar properties is the use of hybrid matrix systems [5]. Interleaving of composite laminates is an established and effective method to improve the fracture toughness of the interfaces [6–8]. A number of approaches, including particles (e.g. thermoplastic polymers) [7,9], films [10–14], or porous but 2D veils, were applied successfully. Electrospun nanofibrous mats are particularly popular and have been widely investigated in recent decades, focusing on mechanical property improvement, as well as aspects related to the manufacturing process [15–20]. The key toughening mechanisms in interleaved thermoset resin based composite laminates include (i) alteration of the brittle nature of the matrix by arresting sharp micro-cracks within soft (micro-) phases before they propagate, (ii) making the interlaminar crack path tortuous by obstructing features and (iii) containment of the interlaminar crack front within a tough interleaf layer. The material systems used for film interleaving are reviewed in [21] and include thermoplastic polymers, which either bond well [11–14] to the matrix of the composite plies (e.g. polyamide 12 (PA12), thermoplastic polyurethane (TPU), polyimide (PI, Kapton) and polyethersulfone (PES)) or can be dissolved in the liquid thermoset resin (e.g. polycaprolactone (PCL) and cardo-polyetherketone (PEK-C)) [22–25]. Fluoropolymer films (e.g. polytetrafluoroethylene (PTFE) or ethylene tetrafluoroethylene (ETFE)) are not suitable for toughening the layer interfaces in composite laminates as they exhibit minimal adhesion to the matrix resins. They are widely used as release films for composite processing and as local crack starters for advanced interfacial property characterisation (e.g., double cantilever beam (DCB) for mode I and end-notched flexure (ENF) for mode II fracture toughness testing). However, perforated fluoropolymer films may be suitable for controlling the adhesion between adjacent composite layers and, therefore, the resulting G_{IIC} of the modified interface. Artificial defects created by the insertion of release film strips into adhesively bonded zones were also

E-mail address: czel.gergely@gpk.bme.hu.

https://doi.org/10.1016/j.compositesa.2026.109743
Received 29 January 2026; Received in revised form 17 March 2026; Accepted 18 March 2026
Available online 19 March 2026

found suitable for mode I and II fracture toughness improvement [26]. Further approaches to improve the toughness of adhesively bonded joints in modes I and II by structuring the joint, e.g., with patterning of the substrate, the adhesive, or the interface between them, can be found in [27].

Despite its apparently detrimental effect on structural integrity, interlaminar weakening may also be considered useful in certain special load scenarios; therefore, an attempt was made to explore early work in this field. A unique application of interleaves as delamination promoters was presented in 1977 [28] to improve the Charpy impact energy absorption of different carbon fibre/epoxy (CF/EP) laminates by aluminium, PA-6, metallised polyester (Mylar), polyquinazoline, Kapton and polycarbonate (PC) film interleaving at multiple interfaces within the samples. Li and Felbeck introduced the concept of *intermittent interlaminar bonding* in 1980 [29]. They used 7 μm thick (~1 mm diameter) perforated Mylar film interleaves with different contact area ratios (18% and 36%) to divert ply fractures into delaminations and improve the translaminar fracture toughness of angle-ply and quasi-isotropic (QI) CF/EP laminates (characterised by compact tension tests). A few years later, perforated Mylar and Kapton films, as well as polyester fibre based thin and porous woven textiles, were also applied in QI glass fibre epoxy (GF/EP) laminates to improve their translaminar fracture toughness and bending properties (under static and impact loading) [30]. Pegoretti et al. [31] interleaved 26 μm thick, 1 mm diameter drill perforated Mylar films to each ply interface of 8 and 16-ply CF/EP orthotropic fabric laminates with the scope of improving the energy absorption in an out-of-plane bending impact load scenario. The effects of interleaving and the contact area ratios applied were assessed using DCB, three-point bending (3 PB), and Charpy impact tests. Relatively good adhesion was obtained between the interleaf film and the composite plies, which was modified by setting the interlaminar contact area (ICA) through the perforation density. The G_{IC} of the laminates was decreased by a factor of 5 by reducing the ICA ratio (ICAR) from 100% to about 2%. The bending strength decreased linearly with decreasing G_{IC}. Energy absorption during Charpy impact tests was significantly improved by reducing the G_{IC} of the ply interfaces, as additional energy was absorbed during the crack propagation phase through multiple delaminations. An optimum G_{IC} was observed at around 80% reduction, where the total impact energy was increased by almost twofold compared to that of the pristine laminates. Kuhtz et al. [32] interleaved rather thick (75 μm) polytetrafluoroethylene (PTFE) films with 4 mm square perforations (turned by 45°, made by a CNC ply cutter with a sharp, oscillating blade) between glass fibre/polypropylene (GF/PP) 3D textile plies and consolidated them in an autoclave. G_{IC} and G_{IIC} values were assessed in relation to the ICAR of the interface modification patterns. The correlation between G_{IC}, G_{IIC}, and the ICAR was reported, and second-order polynomials were fitted to the test data. Quasi-static 3 PB material properties (maximum force and fracture energy) of 16-ply laminates interleaved at all ply interfaces showed a monotonic increase with ICAR. The type of correlation was not obvious from the presented diagrams for mode II. Kuhtz et al. [33] also assessed the impact energy absorption characteristics of CF/EP fabric and GF/PP 3D textile based composites in the function of ICAR. Charpy tests executed on a drop-weight tower indicated that controlled delamination can help reduce fibre fractures and preserve the in-plane structural integrity of the tested materials. In the case of CF/EP samples, the energy absorption capacity was increased by 65% for 60% ICAR for a 24 mm support span, where the shear stresses were more dominant than in the 60 mm span configuration.

The available literature indicates a clear scope for interfacial weakening to improve energy absorption in dynamic load scenarios. The approach was also successfully applied to control damage type and location. Interfacial weakening was realised by (i) full interleaving with a film showing significant adhesion to the surrounding composite layers or (ii) by the *intermittent interlaminar bonding* concept, where the interleaf film with limited or no adhesion to the composite layers was perforated to facilitate direct contact at a given area of the interface. The latter method offers more scope for controlling the reduction of interfacial properties through different perforation pattern designs. The available data is scattered in terms of base materials (i.e., CF/EP, GF/EP, GF/PP) as well as interleaf film materials (mainly Mylar, Kapton, and PTFE), perforation geometry (circular and square shapes), and perforation method (e.g., drilling, CNC cutting). There is also a lack of assessment of perforation patterns to account for possible manufacturing-related deviations from the original design.

The present study aims to systematically investigate the effect of the intermittent interlaminar bonding concept on the G_{IIC} of thermoset matrix composite interfaces, as this is the most relevant property that plays a key role in the design for structural applications. The simplest UD reinforcement type with the most reproducible prepreg curing in autoclave technology was selected to achieve planar interfaces and exclude structural effects reported as potential contributors to interface properties. A flexible laser-cutting-based perforation method was chosen (for the first time in the literature) to enable the analysis of several engineered patterns on a thin, low-adhesion fluoropolymer release film to simplify the potential crack-propagation phenomena at the modified interfaces. A thorough optical analysis of the cut patterns was performed for the first time in the literature to understand the process-related reasons for possible inaccuracies. The further scope of this study is to control the damage location of high-performance composite laminates under static and dynamic out-of-plane loading. Interface modification at selected interfaces of laminates, applied to an engineered extent (e.g., organised patches or local modifications at key areas), seems promising for increasing the total absorbed energy in impact load scenarios and for controlling the location and area of delamination. Increased post-impact in-plane structural integrity and overall durability are also potential benefits of engineered interfacial weakening of composite laminates.

2. Concept and perforation pattern design considerations

The key objective of the study is to develop an interleaving-based technique that can reduce the G_{IIC} of composite interfaces in a well-controlled manner. For example, delamination damage due to out-of-plane overload may be concentrated at the midplane of a laminate using selective interfacial weakening. This way, the relatively high stiffness of the two thick blocks separated by the promoted delamination may improve the post-overload buckling behaviour of the plate under in-plane compression compared to the scenario with the usual delamination pattern (i.e. multiple delaminations spread across the thickness).

The simplest approach is to use a film of a material that shows minimal adhesion to the cured epoxy matrix of the composite plies. Fluoropolymer release films have been extensively experimented with for decades and have also established themselves in standard test methods, e.g., as crack starters. Therefore, a 15 μm thick ETFE release film (Vabatec RF7) was chosen for the experiments. ETFE falls within the range of fluoropolymers, with a moderate maximum application temperature (210-260°C, depending on the actual product and manufacturer), but exhibits excellent “non-stick” properties similar to those of fluorinated ethylene propylene (FEP) and PTFE, which can be applied at even higher temperatures. Full coverage of an area with release film aims to eliminate any adhesion between two neighbouring composite plies, which is useful when a pre-crack must be created. However, the objective here is to preserve a reduced level of adhesion through the interleaf, which may be achieved by cutting designed perforations, e.g., by laser. The matrix of the composite plies can establish full cohesion through the perforations, and the size, shape and pattern of the cuts can be tailored to achieve the targeted G_{IIC}. In this study, the aim was to assess the concept, therefore simple configurations with a thin film (significantly thinner than those in [31–33]) were preferred to minimise the potential disruption to the laminate structure. The most basic shape, circular perforations were cut in a simple quadratic pattern (see Fig. 1. a) with two different nominal diameters: 1 and 1.5 mm. The interlaminar

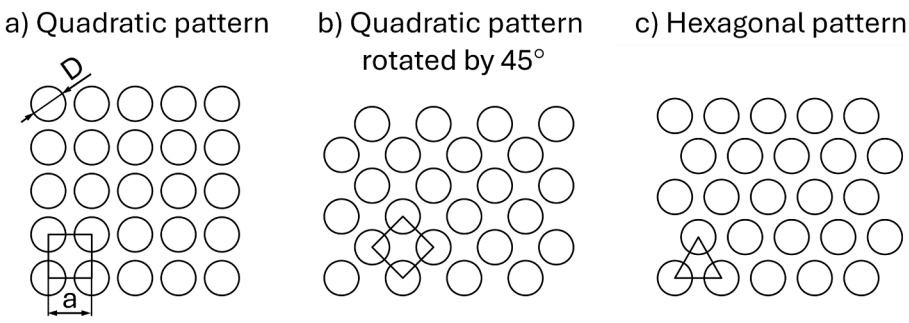

Fig. 1. Possible simple perforation patterns with an interlaminar contact area ratio (ICAR) of 0.5 and their repeating units.

contact area ratio (ICAR) of the interleaf was defined as

$$ICAR = \frac{A_{PERF}}{A_{TOT}} = \frac{D^2\pi}{4a^2} \tag{1}$$

where A_{TOT} is the total area of the representative element, A_{PERF} is the area of the perforation(s) within the representative element, D is the diameter of the circular perforations, and a is the size of the representative element (centre offset for pattern generation, see Fig. 1. a). The centre offset parameter a is required to enable the generation of patterns with variable ICARs. Therefore, a simple formula was derived for it in terms of the circle diameter D and the desired ICAR, based on Equation (1).

$$a = \sqrt{\frac{\frac{D^2\pi}{4}}{ICAR}} = \sqrt{\frac{D^2\pi}{4(ICAR)}} \tag{2}$$

Fabricating high-ICAR perforation patterns was challenging, as the remaining film width became very low (down to 0.38 mm for a 1.5 mm diameter and ICAR = 0.5). Therefore, the highest nominal ICAR for the experiments was set at 0.5. It was noted that a hexagonal pattern (see Fig. 1. c) could be useful if the target ICAR is above 0.5, as it allows up to 36% wider film sections between the circular perforations regardless of the ICAR and diameter. Since the target ICAR in this study was well below 0.5, the quadratic pattern was chosen as it is slightly simpler to generate. Another potentially useful feature of the selected pattern type is that it contains larger "patches" covered with the film between the cuts, which might promote the G_{IIC} reduction effect. The quadratic perforation patterns were turned by 45° to avoid the formation of continuous release film strips in the loading direction (see Fig. 1. b). The actual appearances of the laser perforation patterns were analysed and compared against the nominal designs in section 7.1. The analysed quadratic perforation patterns are summarised in Table 1. Larger, 1.5 mm perforations were selected to study the dependence of G_{IIC} on the ICAR, as they are relatively simple to cut with a laser. Smaller, 1 mm diameter perforations were tested in a second step, as they are preferable due to their more dispersed structure and reduced interference with the geometrical features of a potential composite product. Since a higher number of low-diameter perforations is required to cover the same area with the same resulting ICAR, a more significant deviation between the nominal and actual ICAR is expected, as some material is burned by the laser around the perimeter of the cuts. Fabrication of 1 mm perforation patterns with the same target ICAR took significantly longer, again because of their longer total cutting paths.

Table 1
Analysed perforation pattern configurations.

Perforation pattern designation	Nominal perforation diameter (D_n)	Nominal interlaminar contact area ratio (ICAR)
	[mm]	[-]
D1.5mmICAR0.2	1.5	0.2
D1.5mmICAR0.3	1.5	0.3
D1.5mmICAR0.4	1.5	0.4
D1.5mmICAR0.5	1.5	0.5
D1.0mmICAR0.2	1	0.2
D1.0mmICAR0.3	1	0.3

3. Materials

The materials considered for design and used in the experiments were UD S-glass fibre/epoxy (GF/EP) prepregs from Hexcel, made with Flite Strand S-glass (Owens Corning) fibres and 913 (Hexcel) aerospace-grade epoxy resin, with a cure temperature of 125°C. Vabatec RF7, a 15 μm thick ETFE release film, was used for interface modification. Some key properties of the materials are summarised in Table 2.

4. Coupon design and geometry

The objective of the mechanical test campaign was to determine the G_{IIC} of the interfaces in laminates containing different interleaves and to compare them with that of the baseline laminate without interleaves. Prinz and Gadke [34], then Wisnom [35] proposed a simple tensile test based alternative to the more complicated but standardised ENF test [36] to determine the G_{IIC} of unidirectional composite laminates. The tensile test based approach, revisited recently by Scalici et al. [37] and also called the transverse crack tension (TCT) test, involves a discontinuous layer in the middle of a symmetric UD plate (see Fig. 2.), which promotes the initiation and propagation of four interlaminar crack fronts, leaving delaminated areas behind. The author applied the tensile test-based G_{IIC} determination approach in previous studies [10,11,17,38,39] and found it advantageous for its simplicity and sufficient agreement with data obtained by material manufacturers using more complex standard test methods. The coupons tested within the study were 15 mm wide, UD prismatic tensile test coupons (see Fig. 2.), with one-third of the composite plies in the centre of the laminate being cut perpendicular to the fibres, and optional interleaves incorporated into the expected delamination areas.

During the design of the coupons, the simple stacking sequence of continuous and discontinuous layers of the same thickness and orientation was checked from two aspects: (i) The preferred strain regime for delamination initiation is above 1% to avoid the initial segment of the stress–strain curve, but delamination should happen well before reaching the failure strain of the continuous GF/EP plies to avoid premature fracture of the coupons. (ii) During the tensile test up to the event of delamination, the continuous layers near the discontinuity need to be able to take the full load, which is carried by all the plies anywhere else along the length of the coupons. The highly loaded section of the continuous plies extends together with the delamination areas. This condition corresponds to a stress concentration factor of 1.5 in the continuous GF/EP layers, initially at the discontinuity and later in the delaminated section.

Table 2
Properties of the applied materials based on the manufacturer's datasheet values.

Fibre type	Manufacturer	Diameter	Elastic modulus	Strain to failure	Tensile strength	Density
		[μm]	[GPa]	[%]	[GPa]	[kg/m^3]
Flite Strand S-glass	Owens Corning	9	92	3.6–4.4	3.3–4.1	2450

Prepreg type	Manufacturer	Nominal fibre areal density[a]	Fibre volume fraction[a]	Nominal cured ply thickness[b]	Predicted elastic modulus[b]	Failure strain
		[g/m^2]	[%]	[mm]	[GPa]	[%]
S-glass fibre/913 epoxy (GF/EP)	Hexcel	305	49	0.25	47.1	3.9[c]

Release film type	Manufacturer	Material	Nominal thickness	Tensile strength (both directions)	Failure strain (machine direction)	Failure strain (cross direction)
			[μm]	[MPa]	[%]	[%]
Vabatec RF7	Vabatec	ETFE	15	>40	>170	>300

[a] Based on the manufacturer's product-specific data.
[b] Estimated using manufacturer's product-specific data.
[c] Conservative average experimental value for design purposes obtained with similar material.

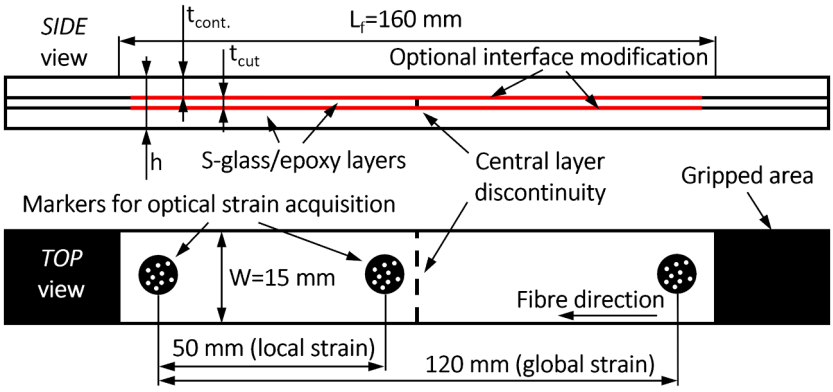

Fig. 2. Schematic of the UD cut central layer tensile test coupons for the determination of G_{IIC}.

A simple formula was presented in [35] and applied here to estimate the mode II energy release rate G_{II} at a given stress in the cut central layer coupons:

$$G_{II} = \frac{\sigma^2 h t_{cut}}{4E(h - t_{cut})} \tag{3}$$

where σ is the stress calculated for the full cross-section of the coupon, h, and t_{cut} are the thicknesses of the coupon and the cut layer, respectively, and E is the elastic modulus of the GF/EP. The formula was converted to strain (ε), assuming a linearly elastic response until delamination initiation, as it was easier to tune the preferred delamination initiation to the failure strain of the GF/EP plies than using stresses affected, e.g. by possible variations in thicknesses:

$$G_{II} = \frac{E\varepsilon^2 h t_{cut}}{4(h - t_{cut})} \tag{4}$$

To fulfil condition (i), G_{II} with the configuration of [0.5 mm continuous/0.5 mm cut/ 0.5 mm continuous] UD GF/EP was checked at 1 and 2% strain and found to be 0.89 and 3.57 N/mm, respectively. Based on previous test results on similar materials [17], delamination initiation was expected to occur somewhere between the analysed strains, and a sufficient margin was left to avoid premature failure of the continuous plies before delamination initiation, as G_{IIC} values below 1 N/mm and above 2 N/mm had never been obtained before.

Condition (ii) was checked, assuming a high 2% strain for delamination initiation and a conservative 3.5% failure strain for the GF/EP based on previous tensile tests on similar material. The previously published formula for CF/EP layers of different moduli [40] was adopted:

$$t_{cont} > \frac{\varepsilon_{del} E t_{cut}}{2E\left(\varepsilon_{bGF/EP} - \varepsilon_{del}\right)} \tag{5}$$

where t_{cont} is the thickness of one continuous layer (see Fig. 2.), ε_{del} is the assumed delamination strain (i.e. 2%), and $\varepsilon_{bGF/EP}$ is the estimated breaking strain of the GF/EP (i.e. 3.5%), t_{cut}=0.5 mm. A minimum of 0.336 mm was obtained for t_{cont}, after substituting the parameters, which provides a sufficient (approx. 50%) margin to the applied 0.5 mm nominal thickness to avoid the premature fracture of the continuous layers in the coupons.

The nominal free and overall length of the coupons were L_f = 160 mm and 260 mm, respectively. The placement of the perforated release film interleaves is presented in Section 5. No end-tabs were bonded on the coupons as the discontinuous plies localised and initiated the mode II delamination damage well before the continuous plies would break. Therefore, the stress concentrations around the grips were not critical, and the coupons were not destroyed but remained in one piece until the tests were terminated.

Please note that the mode I interfacial fracture toughness G_{IC} of the modified interfaces is also expected to be influenced by the perforated release film interleaves, but a less straightforward correlation between the ICAR and the G_{IC} is expected, as the layer separation effect of the perforated release films may hinder some mechanisms (such as fibre

bridging). Since mode I fracture properties play an important role, e.g., during unloading or post-impact buckling load scenarios, the author believes that their characterisation in perforated release film modified laminates deserves attention for further investigation.

5. Composite plate manufacturing and coupon fabrication

GF/EP composite laminates were manufactured by manually stacking six 300x300 mm plies of UD prepreg with the same orientation, according to Fig. 2. (longitudinal section showing the layer discontinuity and interface modification areas) and Fig. 3. (showing the position of the same features in top view). The author [41] had previously experienced that UD laminates do not have flat ply interfaces but exhibit out-of-plane widthwise ply undulations in their cross-sections perpendicular to the fibres. This effect may influence the mode II fracture process of UD laminates, therefore an attempt was made to flatten those interfaces within the laminates, which were selected for further modification. Flat interfaces are desired as the G_{IIC} modification approach is planned to be implemented in multi-directional laminates, where the ply (or ply block) interfaces are inherently flatter, as no fibre bundle nesting occurs due to different fibre orientations in the adjacent layers. The ply block flattening technique is explained step-by-step: (i) Three blocks of double plies wrapped in release film were stacked on a flat Al tool plate with 5 mm thick flat Al plates between and on top of them. (ii) The whole stack of three double-ply blocks and three Al plates was put under vacuum on a tool plate in a bag similar to those used for autoclave curing and heated to approximately 60°C in a convection oven to soften the epoxy resin in the prepreg plies. (iii) The stack of ply blocks and flat plates was cooled down to room temperature under vacuum, and then the ply blocks were laid up into laminates as usual. The ply blocks became notably flatter after the combined heat and vacuum treatment, allowing the fabrication of two baseline laminate types (i.e., pristine and flattened) and the assessment of the effect of out-of-plane waviness in the UD composite layers on the G_{IIC} of the laminates. The interleaved laminates were made of flattened ply blocks to minimise the variability in their G_{IIC}.

The test plates were prepared in the following steps: (i) Two UD plies were stacked in a block together with the optional perforated release film pieces on both sides and cut perpendicular to the fibres with a rotary blade to form the central ply block of the laminate, according to Fig. 3. (ii) Two further blocks of two continuous UD plies were prepared. (iii) The ply blocks and the optional perforated release film pieces were stacked into one laminate with the same fibre orientation according to the side view schematic of Fig. 3 with the following order: [continuous ply block/optional interface modification/ply block with cut/optional interface modification/continuous ply block]. The prepared prepreg stacks were fully wrapped in release film, and sufficiently thick silicone strips were placed around them on an Al tool plate to minimise resin bleed-out from the plies. 5 mm thick Al top plates were used to reduce the thickness variation of the cured GF/EP plates. The laminates were then vacuum bagged and cured in an autoclave (Olmar ATV 1100/2000) for 60 min at 125°C and 7 bar pressure (as recommended by the manufacturer). Individual coupons were cut from the cured test plates using a Mutronic Diadisc 5200-type precision cutter with a diamond particle-coated wheel.

The effect of ply block flattening was assessed on polished cross-sections of cured baseline laminate samples using a Keyence VHX-5000 digital microscope with a VH-Z100UT VH zoom lens. The samples were cast into transparent epoxy resin and polished on a Buehler Beta machine using the following abrasive sequence: P400 grit SiC paper, 9 μm and 3 μm diamond suspensions, and finally a 0.05 μm alumina suspension, all supplied by Buehler. Fig. 4 shows the result of an attempt to manually track the ply block interfaces on high-resolution mosaic images.

The figure suggests only marginal differences between the shapes of the layer interfaces, but confirms that the extra step in the manufacturing process helped consolidate the plies slightly better.

6. Mechanical test method

Testing of the coupons was executed under uniaxial quasi-static tensile loading and displacement control at a crosshead speed of 5 mm/min (total test time 100–200 s) on a computer-controlled Zwick Z250 type 250 kN rated universal electro-mechanical test machine fitted with a regularly calibrated 250 kN load cell and 100 kN rated Instron 2716–003 type manual wedge-action grips. The strains were measured optically on one side of the coupons using a Mercury Monet type video-extensometer with two 5-megapixel resolution cameras to cancel the possible effect of out-of-plane displacements of the coupons. Two different sections were prepared for optical strain measurement

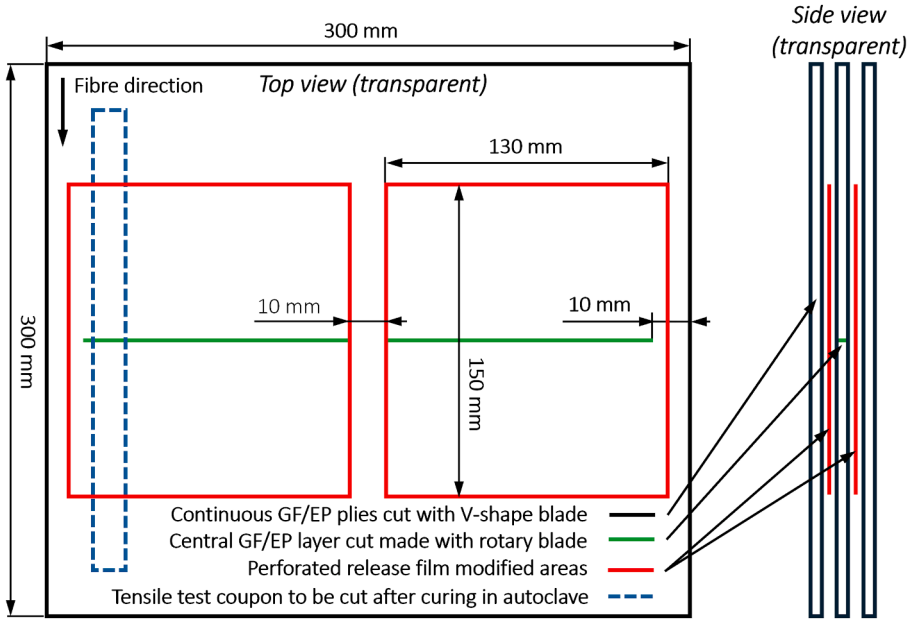

Fig. 3. Schematic of the position of cut lines and components used for the fabrication of interface-modified composite plates.

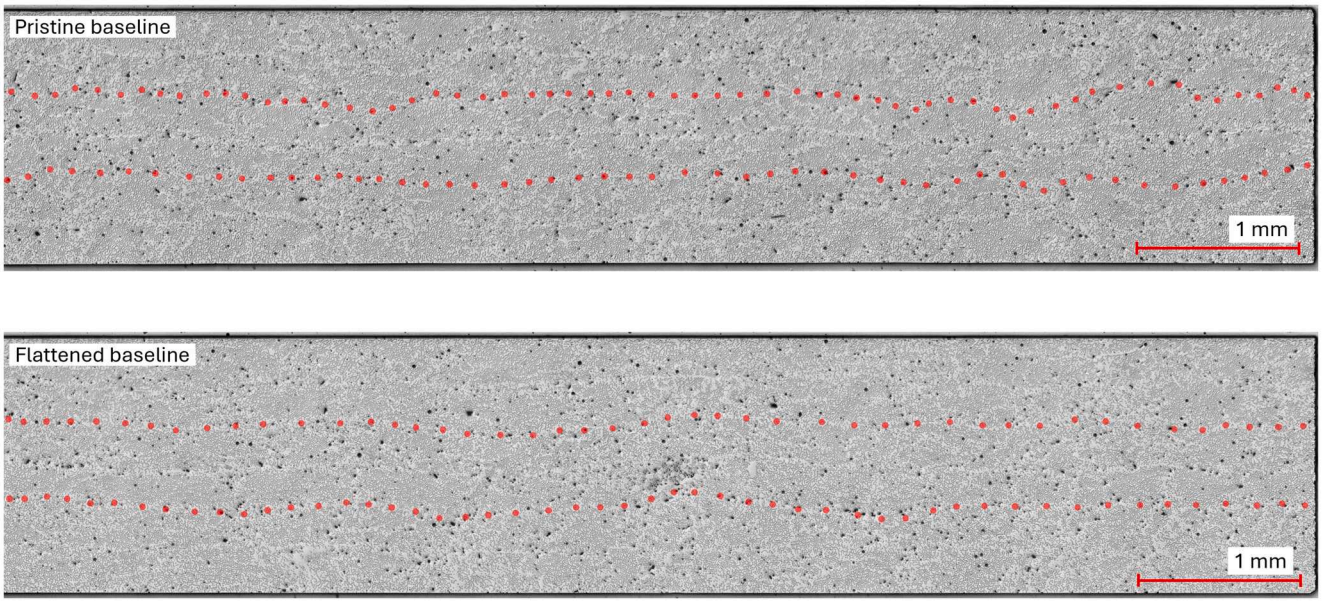

Fig. 4. Digital microscope images of the polished cross-sections of baseline laminate samples with dots showing the anticipated positions of the interfaces between blocks of double plies.

(see Fig. 2), creating high-contrast targets of white dots (with a sharp-tip paint marker) on a black background (with a blunt-tip permanent marker). The longer, approx. 120 mm section included the central layer discontinuity zone, while the shorter, approximately 50 mm section was designed to exclude it. This specialised strain measurement setup enables the assessment of the effect of the central discontinuity on the overall stress–strain response.

7. Results and discussion

7.1. Assessment of the perforation patterns

The ETFE release films were cut using a Versa Laser VLS2.30 type cutting/engraving CO_2 laser with a 10.6 μm wavelength and a maximum power of 30 W. Since the control software of the laser cutter did not allow precise setting of the cutting parameters, the power and the speed of the laser beam were assessed during a series of preliminary trials and the optimal settings were used throughout the rest of the study. Plain A4 sheets of paper were placed under the thin ETFE films to support them over the metallic honeycomb table of the cutter. The laser was set to cut the film fully, but not to cut through the paper, leaving only marks. The "strength" (i.e., darkness and width) of the burnt marks on the backing paper was helpful in assessing the optimal power and speed of the laser beam, which are opposing parameters. Maximum speed and sufficient power were targeted to reduce the fabrication time.

The different perforation patterns of the release film samples (see Table 1) were analysed with a Keyence IM-7020 type image dimension measurement system featuring a 1-inch, 6.6 megapixel monochrome CMOS sensor (see Fig. 5a.) to assess the geometrical precision of the fabricated perforation patterns through comparison to the original design (nominal values). The achievable measurement repeatability and accuracy were ± 2 and ± 5 μm, respectively. The diameters and centre positions of the circular perforations were determined using the contour and shape recognition capabilities of the measurement system. A convenient 5x5 circle area was analysed to reduce the effect of one-off defects (see Fig. 5b.), and the parameters A_{TOT} and A_{PERF} were

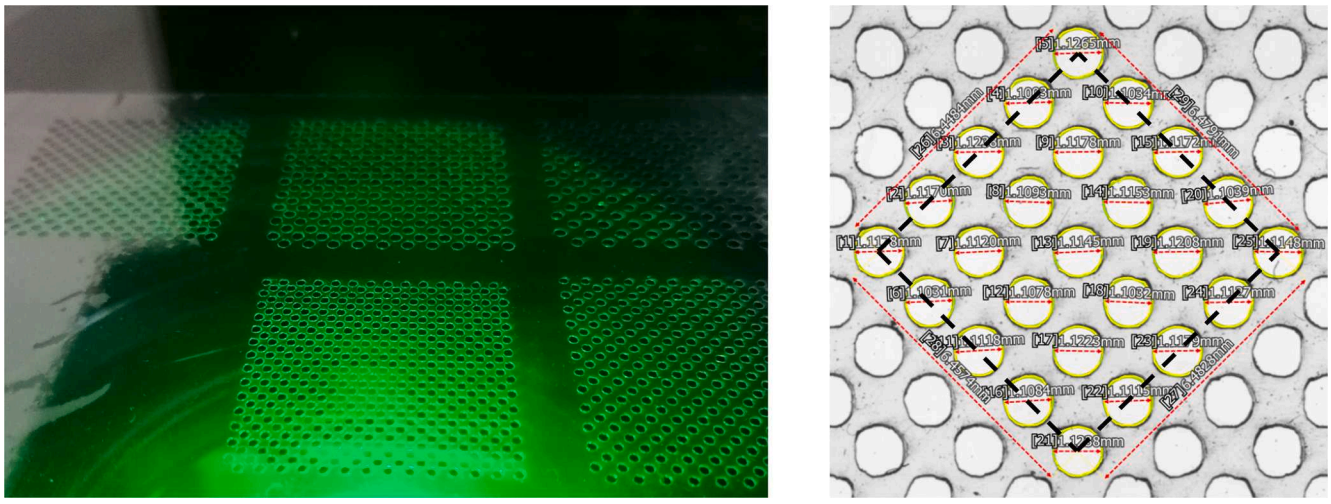

Fig. 5. a) Samples on the table of the image dimension measurement system, b) processed image taken by the measurement system from a D1.0mmICAR0.3 type sample (black dashed lines showing the region of interest).

Table 3
Results of the optical assessment of the perforation patterns. (ICAR: interlaminar contact area ratio, values in brackets correspond to the coefficients of variation (CoV) of the average parameters in [rel.%]).

	Nominal diameter (D_n)	Measured average diameter (D)	Absolute/relative difference in diameter	Nominal ICAR	Average ICAR calculated from measured data	Difference in ICAR	Total perforation length* to cover 100 mm^2
	[mm]	[mm]	[mm] / [%]	[-]	[-]	[-]	[mm]
D1.5mmICAR0.2	1.5	1.617 (0.62)	0.117/7.819	0.2	0.233	0.033	53.3
D1.5mmICAR0.3	1.5	1.607 (0.69)	0.107/7.140	0.3	0.344	0.044	80.0
D1.5mmICAR0.4	1.5	1.607 (0.72)	0.107/7.159	0.4	0.456	0.056	106.7
D1.5mmICAR0.5	1.5	1.581 (0.79)	0.081/5.405	0.5	0.557	0.057	133.3
D1mmICAR0.2	1	1.113 (0.97)	0.113/11.25	0.2	0.248	0.048	80.0
D1mmICAR0.3	1	1.114 (0.67)	0.114/11.38	0.3	0.373	0.073	120.0

*Calculated with the nominal perforation diameters, as those are more relevant to cutting route generation.

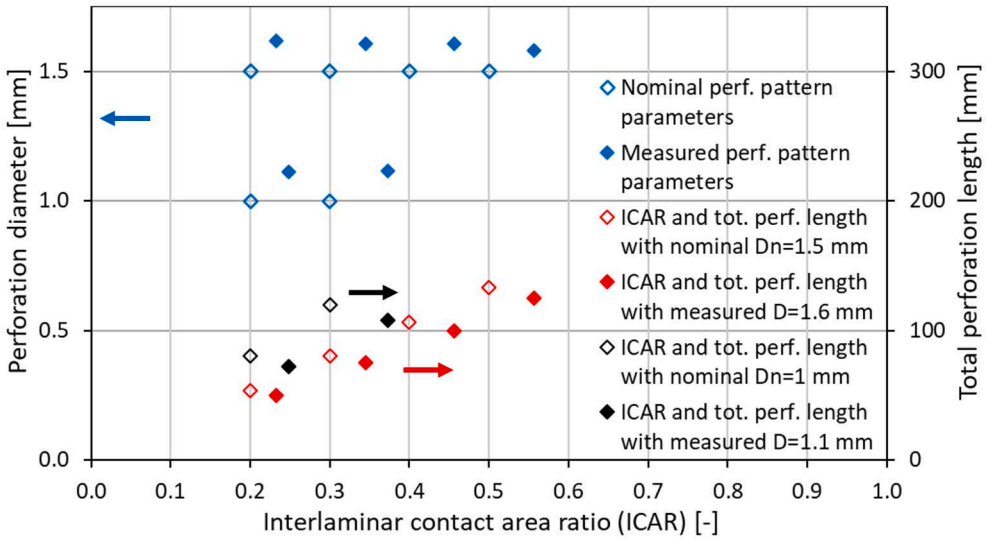

Fig. 6. Nominal and measured parameters of the investigated perforation patterns and total perforation lengths calculated with the nominal and measured parameters to cover 100 mm^2 (Dn stands for nominal diameter).

calculated based on the measured edge sizes of the region of interest and the individually measured circle diameters.

Table 3 and Fig. 6 show the results of the optical measurements in comparison to the nominal values. Circle diameters were measured individually for 25 circles in each configuration, and average ICAR values were obtained from sufficiently large regions of interest (see Fig. 5b). The measured diameters are approximately 0.1 mm larger than the nominal values (regardless of the set nominal diameter), which represents a larger relative difference (up to 11%) in the case of the lower, 1 mm nominal diameter circles. The observed approximately constant increase in the resulting diameter was expected, as the laser beam has a finite width and burns some material while cutting. The recorded diameter differences provide a basis for compensating for the exact route input to the cutting machine. However, the required compensation is expected to be specific to a given piece of equipment and cutting parameters, therefore no further steps were taken to get closer to the nominal diameter.

The actual ICAR values show differences of up to 0.07 from the nominal ones, with an increasing trend towards higher targeted ICARs (see Fig. 7). This was expected, as more circular perforations and a longer total perforation length are required to cover the same area with a higher ICAR pattern. Higher differences are observed for lower diameter patterns for the same ICAR, as the deviation is associated with the total length of the cutting route (see Fig. 7), which is up to 15% higher for the patterns with 1 mm than for the 1.5 mm circles based on a simple geometric calculation. Visual assessment of Fig. 7 confirms monotonic trends between the total perforation length and the difference between the nominal and measured ICAR values of the assessed perforation pattern configurations. The calculated total perforation length values (based on the nominal perforation diameters, which are more relevant to cutting route generation) to cover an arbitrary 100 mm^2 area are included in Table 3 and Fig. 6, as well to aid in explaining the trends observed in the measured data. The designations of the laminate configurations featuring interfacial modification have been updated according to the test results and will be used in the new form during the discussion of the mechanical test results.

7.2. *Mode II fracture toughness test results*

The scope of this section is to compare the G_{IIC} of the laminates modified with perforated release film interleaves to those of the two different type (i.e. pristine and flattened) baseline laminates. The tensile stress–strain responses of the coupons were recorded and used to evaluate their G_{IIC}, therefore these are discussed first. As explained in Section 6 and presented in Fig. 2, the stress–strain diagrams of the individual coupons were recorded in two ways, including and excluding the central

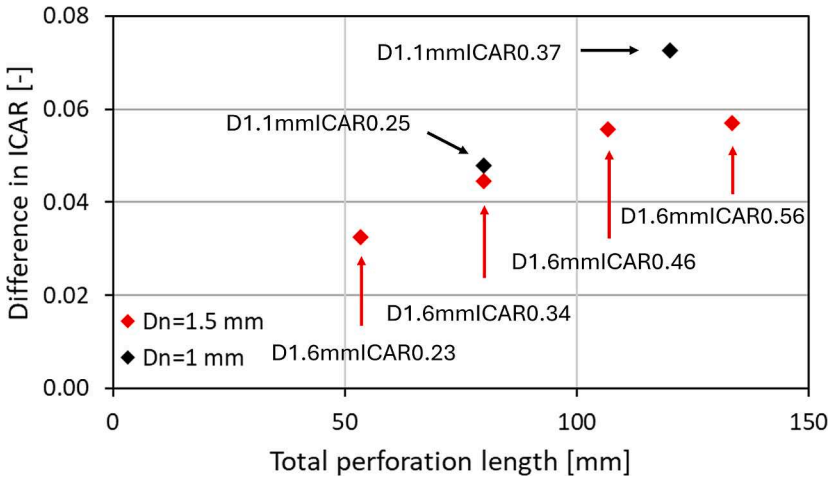

Fig. 7. Increase of the observed difference in the interlaminar contact area ratio (ICAR) in function of the total perforation length for the assessed perforation pattern configurations. (Total perforation length values were calculated for a 100 mm^2 area using the nominal perforation diameters, as it is more relevant to cutting route generation; Dn stands for nominal diameter).

layer discontinuity zone using the global- and local strain recordings, respectively (see Fig. 8). The local- and global strain based responses started to deviate from around 0.6% strain visibly in case of the presented curves. This deviation typically began later in cases of other configurations with less severe interfacial modification, but became visible around the strain of 1% at the latest. The coupon in Fig. 8 showed an outstanding extra strain of up to 0.2% (global vs. local) due to delamination initiation around the central layer discontinuity before unstable delamination propagation. In the case of the other configurations, the observed extra strain was usually smaller, but the local strain values recorded on a section excluding the central layer discontinuity were selected for further evaluation and presentation, as they are less affected by strain variations. In the rest of the manuscript, "strain" refers to the specific elongation measured over an approx. 50 mm long section, excluding the middle zone of the coupons where the central layer is discontinuous (i.e. the local strain in Fig. 8.).

The G_{IIC} of the interfaces in the coupons were evaluated both based on stress (equation (3)) and strain (equation (4)), taking the last point before the stress drops associated with delamination into account. Since the difference was minor, a stress-based evaluation was selected to present the results (see Table 4), as delamination propagation typically occurs at a constant stress, enabling a more accurate G_{IIC} evaluation. Delamination propagated unstably in most coupons, but traces of a plateau on the stress–strain diagram were observed in a few cases (e.g., for the one in Fig. 8).

Fig. 9 shows the stress–strain responses of the tested coupon series. The diagrams confirm that the test data for each series are consistent and show limited scatter. The elastic modulus of all series was similar within the experimental scatter (43 GPa on average) but up to 10% lower than the predicted value (47.1 GPa) based on the prepreg manufacturer's data. The layer discontinuity was expected to contribute slightly to the observed reduction in elastic modulus. Most of the coupons delaminated suddenly, and the corresponding stress drops are clearly visible on the individual stress–strain diagrams, facilitating the simple and accurate

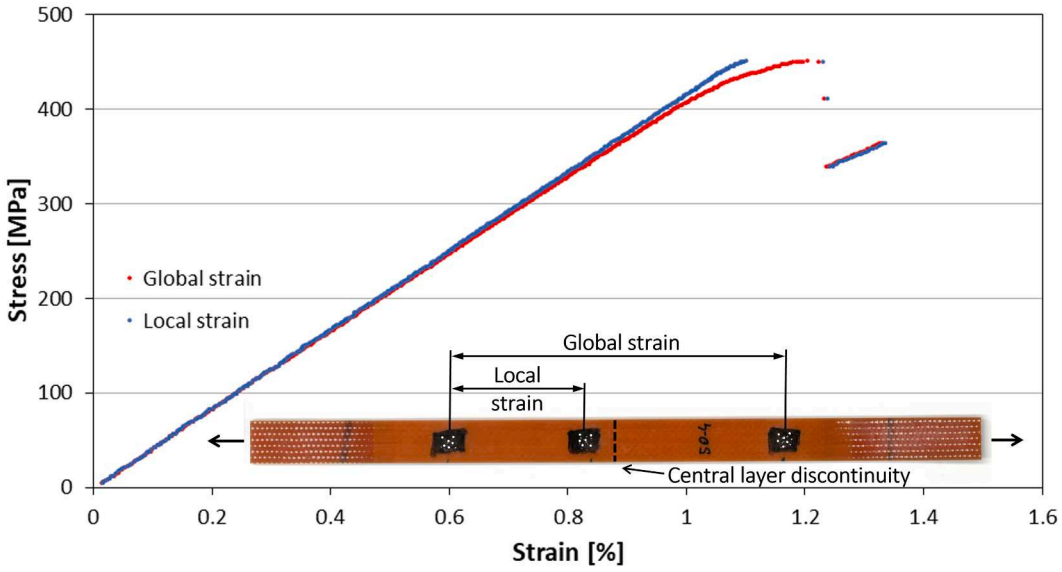

Fig. 8. Comparison of the stress–strain diagrams of a D1.1mmICAR0.25 coupon showing a short plateau before delamination. Data was recorded using longer (global) and shorter (local) gauge sections for strain acquisition.

Table 4
Results summary of the tensile tests. (Values in brackets correspond to the coefficients of variation (CoV) of the average parameters in [rel.%]. The cut layer thickness was estimated by taking one-third of the total measured thickness. Please note that specimen designations were updated based on the optical assessment of the pattern geometries).

	Measured width (W)	Total measured thickness (h)	Estimated cut layer thickness (t_{cut})	Elastic modulus (E)	Delamination stress	Delamination strain	G_{IIC} from stress	Relative difference in G_{IIC}*
	[mm]	[mm]	[mm]	[GPa]	[MPa]	[%]	[N/mm]	[%]
Baseline	15.02	1.51	0.503	43.53	673.3	1.564	1.968	5.37
	(0.14)	(0.70)		(1.34)	(3.00)	(4.04)	(7.24)	
Flattened baseline	15.03	1.47	0.491	43.74	665.9	1.542	1.868	–
	(0.07)	(1.67)		(1.53)	(1.72)	(1.42)	(2.96)	
D1.6mmICAR0.34	15.04	1.49	0.497	42.54	522.2	1.237	1.194	−36.08
	(0.08)	(3.40)		(1.55)	(1.94)	(2.81)	(3.39)	
D1.6mmICAR0.46	15.04	1.54	0.512	42.98	605.0	1.424	1.634	−12.52
	(0.08)	(0.81)		(0.93)	(1.16)	(1.38)	(1.74)	
D1.6mmICAR0.56	15.04	1.52	0.507	43.38	684.9	1.598	2.056	10.07
	(0.05)	(0.95)		(0.93)	(1.90)	(1.66)	(3.60)	
D1.1mmICAR0.25	15.06	1.52	0.506	42.49	456.8	1.087	0.932	−50.11
	(0.11)	(1.40)		(1.15)	(2.67)	(3.57)	(4.73)	
D1.1mmICAR0.37	15.07	1.52	0.507	42.30	549.8	1.315	1.359	−27.26
	(0.10)	(1.14)		(1.70)	(1.57)	(0.81)	(1.61)	

*Compared to the average G_{IIC} of the flattened baseline series.

evaluation of the G_{IIC} using the last reliable stress value before the drop and equation (3). As a general trend across all laminate configurations in Fig. 9, a reduction in the maximum stress (and strain before the load drop) was observed with decreasing ICAR. This trend was clearly translated to a reduction in G_{IIC} with decreasing ICAR (see Fig. 10).

The average G_{IIC} of the pristine and flattened baseline coupons in Fig. 10 shows a difference of more than 5%, but their scatter bands overlap significantly. A two-sample Student's t-test with two-tailed distribution, considering unequal variances (also called the Welch-test), was applied to assess if the observed difference is statistically significant. A p-value of 0.155 was obtained, indicating that the probability of the average values being different is less than 85%. This is not considered sufficient for statistical significance, but it suggests a slight decrease in G_{IIC} due to the flattening of the delaminating layer interfaces. This difference was expected, as undulated ply interfaces may increase the energy required for mode II crack propagation by mechanical interlocking due to fibre bundle nesting. The CoV of the pristine baseline series was significantly larger than that of the other series, inc. the flattened baseline one (see Table 4. for details). Flattening of the layer interfaces appears to result in more consistent G_{IIC} values.

It is interesting to note that the laminate with an ICAR of 0.56 showed a higher average G_{IIC} than those of both baseline laminates, however the difference is only statistically significant compared to the more relevant flattened baseline (with a p-value of 0.0007 based on the Welch test). This indicates that the positive effect of the structured adhesion pattern through the perforations was stronger than the effect of having no adhesion at 44% of the layer interface area. The interface modification could have hindered the mode II delamination propagation by the details of the perforation patterns, which may have eliminated the stress singularities that can develop easily at wide, straight crack fronts. This hypothesis was further investigated in Section 7.3. by exploring the fracture surface morphology of the delaminated interfaces of tested coupons. Since the total thickness of the laminates did not increase significantly for any of the perforation patterns, the approach may be considered for the limited but well-controlled increase of G_{IIC} for structural applications. Analysis of mode I fracture performance is essential if perforated film interleaving is considered for toughness enhancement, as some mechanisms (e.g. fibre bridging) may be hindered in opening mode.

The key finding of the experimental study is that the G_{IIC} values of the laminate configurations made with 1.5 mm nominal diameter perforations in the interleaf films follow a very strong linear trend with increasing ICAR ($R^2 = 0.999$) over the studied range. This explored trend, together with findings describing the key features of inaccuracies in laser perforations, enables the accurate prediction, design, and control of the G_{IIC} of layer interfaces in composite laminates. Fig. 10 shows the G_{IIC} values presented in [33] for fabric-based CF/EP with thick (75 μm) interleaves and large, 4 mm square perforations. The G_{IIC} values reported by Khutz et al. [33] were significantly lower for similar ICARs. This difference was mainly attributed to the different reinforcement structure (i.e. UD vs fabric), different matrix material, different perforated release film thickness (15 μm vs 75 μm) and different perforation pattern geometry (1–1.5 mm round vs 4 mm square). Still, the contribution of the applied different test methods (UD cut central layer tensile vs ENF) to the observed differences in the G_{IIC} values cannot be ruled out. Regardless of the different base materials, interleaf film materials, and interleaf configurations, Khutz et al. also reported a monotonic increasing trend. However, the exact trend up to an ICAR = 1 is unclear due to missing data in the high-ICAR regime, where it becomes extremely hard or even impossible to prepare the perforated release film because of very narrow remaining film sections between the perforations. Nevertheless, a strong linear trend was confirmed in both studies in the ICAR regime, which is of practical relevance. This indicates the universal effect of the intermittent interlaminar bonding concept on the G_{IIC} of thermosetting composite layer interfaces. The scope of using the 1 mm nominal diameter configurations in the present study was to apply smaller perforations, which are expected to be more dispersed (i.e. less disruptive to the laminate structure) and to find a suitable ICAR, which leads to approximately 50% G_{IIC} reduction. It is interesting to note that perforation patterns with the same ICAR but lower hole diameters are expected to result in slightly higher G_{IIC}, according to Fig. 10. The most probable reason for this is that having a higher number of small disruptive features (i.e. perforations) makes the crack paths slightly more tortuous and therefore may increase the fracture toughness. The configurations D1.1mmICAR0.25 and D1.1mmICAR0.37, having nominal ICARs of 0.2 and 0.3, were found suitable for further application in quasi-isotropic laminates to concentrate delamination damage to specific interfaces under static indentation.

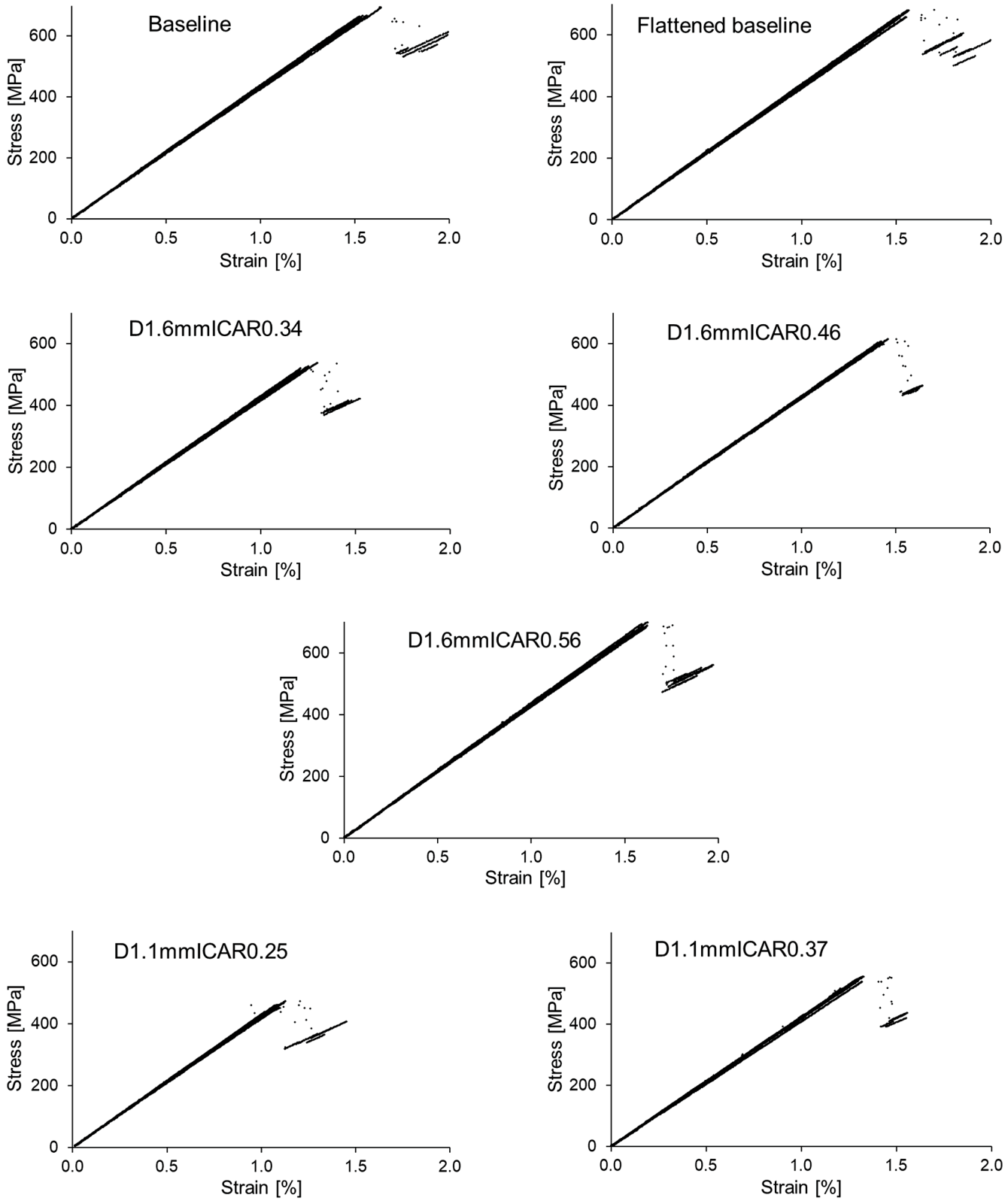

Fig. 9. Aggregated tensile stress–strain responses of the investigated laminate configurations.

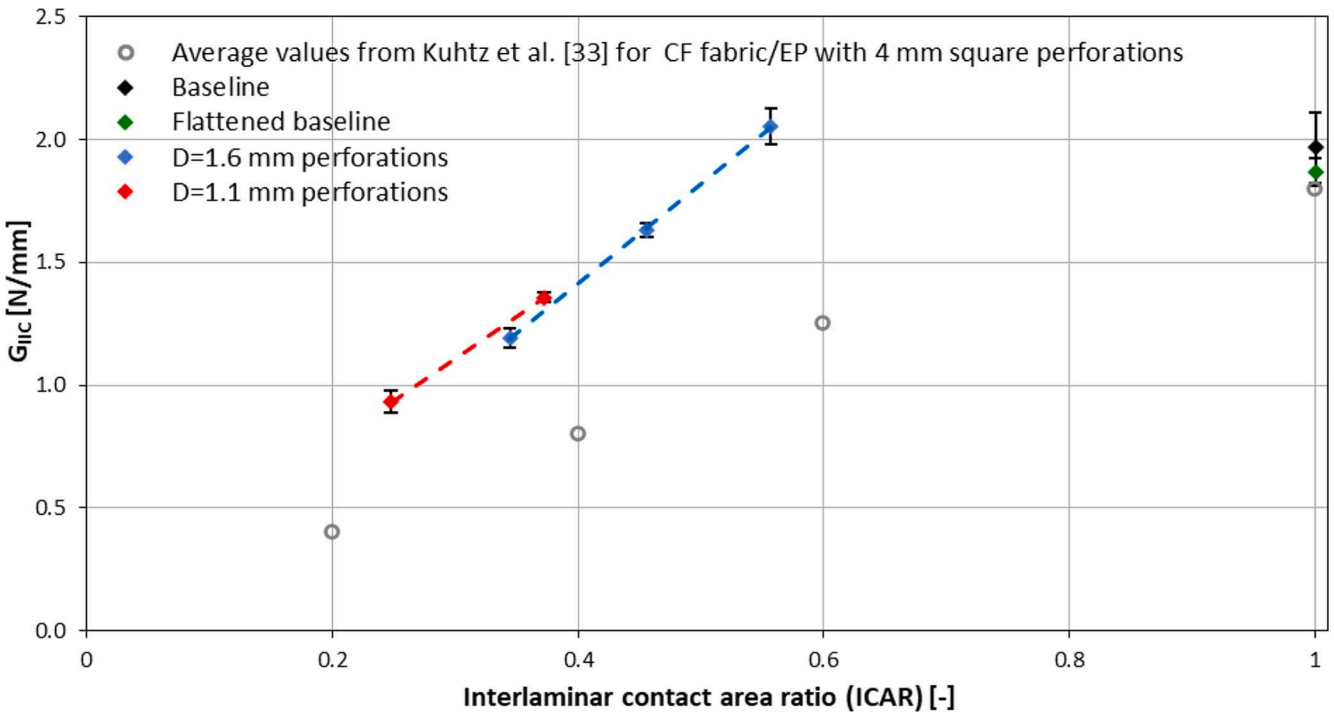

Fig. 10. G_{IIC} results summary of the investigated UD GF/EP configurations, including data from [33] obtained for CF fabric/EP with 4 mm square perforations.

7.3. Delamination fracture surface analysis

Microscopy techniques were utilised to understand the structure of delaminated interfaces and the damage mechanisms active during the mode II fracture of the layer interfaces in the tensile test coupons. Mosaic images were captured with a digital microscope (Keyence VHX-5000 with VH-Z100UT VH zoom lens) to assess the overall appearance of the fracture surfaces of the interface-modified laminates after mode II delamination. This technique was chosen for the initial observations because it requires minimal sample preparation. Samples were cut with the precision cutter equipment used for fabricating the tensile test coupons, and were taken from the central section of the tensile test coupons immediately next to the artificial discontinuity in the central layer. The perforated release film was consistently found on the central ply block side of the delaminated interfaces, as expected, since the perforated release film pieces were cut together with the central ply blocks during the lay-up procedure. Therefore, the overall appearance of the interfaces was first investigated on pieces of the central ply blocks, which easily fell out of the tested coupons after cutting them across the fibre direction approximately 20 mm away from the central ply block cut. Fig. 11. shows the typical overall appearance of the central layer interface of a D1.6mmICAR0.34 type sample with the perforated release film on it (referred to as the film side of the interface). The close-up views suggest that partially exposed fibres are present on the surface of the epoxy layer at the perforations, and that they are broken around the perimeter of the circular perforations through the release film. The other two investigated samples (i.e. D1.6mmICAR0.56 and D1.1mmICAR0.25) showed very similar damage patterns.

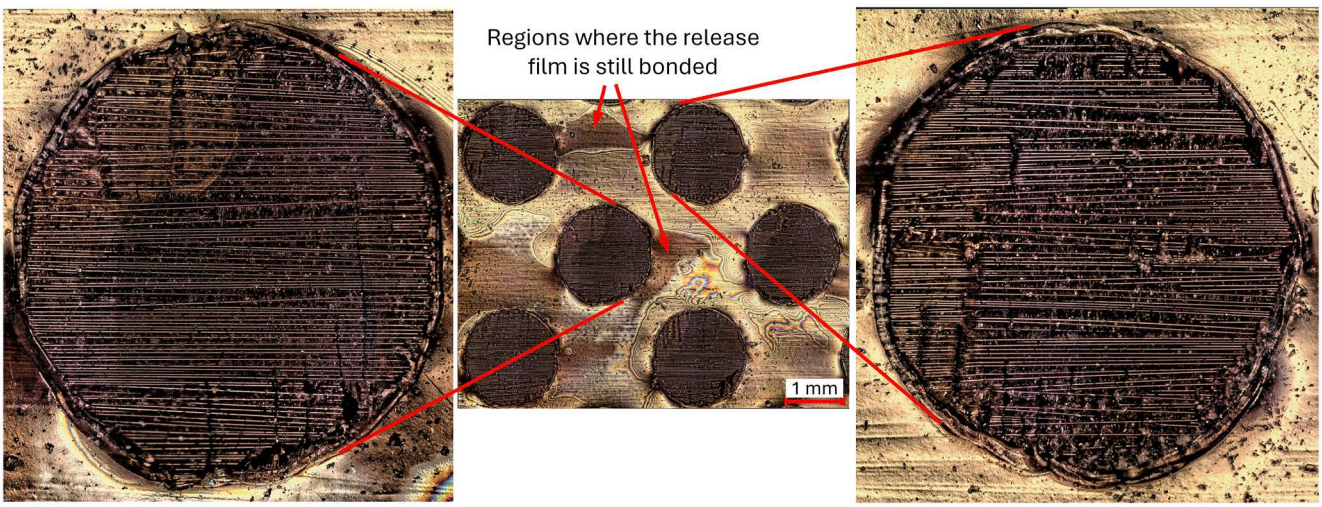

Fig. 11. Overall view of the delaminated interface of a D1.6mmICAR0.34 type sample with the release film around the circular perforations (film side of the interface). Close-up views suggest the presence of exposed fibres broken around the perimeter of the perforations.

Lighter and darker areas in Fig. 11 around the perforations indicate that the release film is no longer fully attached to the composite layer (the lighter areas are detached, while the darker regions are bonded). Since the magnification and resolution of the digital microscope images were found insufficient for detailed analysis of the fracture surfaces, a comprehensive scanning electron microscope (SEM) analysis was conducted (with a Jeol JSM 6380LA equipment using the secondary electron detector) to explore the dominant damage modes at the delaminated interfaces of selected coupon types. Images from different coupon types (as indicated in the figure captions) are presented in the following section to demonstrate that the observed features were very similar across all perforation patterns. Samples cut from the tested coupons were sonicated in a water bath to remove the residual dust, dried and sputter-coated with gold to eliminate static charging. The SEM images in Fig. 12 show the typical appearance of the film side of the delaminated interfaces and reveal that there are no fibres (as assumed based on Fig. 11), only traces of fibres at the surface in the perforation zones.

Fig. 13 shows the two sides of a debonded epoxy block that joins the adjacent composite layers via a perforation in the release film. The debonded fibres are clearly visible on the no-film side of the interface. Although epoxy pieces broken off from the resin-rich layers outside the perforation zones were uncommon in the investigated samples, this particular site was found helpful for visualising the structure of the fractured modified interfaces. In all samples, resin blocks with traces of fibres stood out on the film side and had their corresponding recesses on the no-film side, revealing the surfaces of densely packed fibres that were left exposed after local debonding during the mode II delamination process (see Fig. 13). The polished cross-section of a pristine D1.1mmICAR0.25 type coupon was studied to understand the structure of the interlayer (formed by the interface modification) and its distinctive damage pattern observed on the SEM images. Fig. 14 reveals that the laser-cut edges of the perforations are uneven and have features (formed by melting and burning) that are significantly thicker than the film itself. These uneven and typically thick laser-cut edges pushed the stiff fibres in the neighbouring composite layers apart, making space for resin pockets at the perforations. Since the perforated release films acted as separators between adjacent composite layers, they retained some excess epoxy at the interface by blocking resin migration and hindering dense fibre packing through nesting. Fig. 14 also demonstrates the appearance of the non-modified ply interfaces within the three ply blocks, whose expected positions are marked on the micrograph but are very hard or impossible to recognise due to resin migration and fibre nesting. The almost invisible ply interfaces confirm that there are no significant resin-rich layers or areas at the non-modified interfaces, just as in the baseline samples (see Fig. 4).

Fig. 13. and Fig. 14. confirm the existence of a structured interlayer (formed between the composite blocks by the insertion of the perforated release films), that did not break along one side of the release film but followed a slightly more tortuous fracture path, inclining towards the interface between the resin pockets at the film perforations and the densely packed fibres on the no-film side. This fracture behaviour is expected, as the interlaminar cracks followed the lowest energy path: epoxy block debonding from a stiff substrate (i.e. densely packed glass fibres) instead of shear fracture of the block.

In contrast, the delaminated interfaces of the baseline samples show a balanced number of debonded fibres and fibre traces (see Fig. 15.), indicating the absence of a distinct resin-rich layer in agreement with the appearance of the analogous ply interfaces on the cross-section micrographs of Fig. 4. and Fig. 14. This appearance is typical in unidirectionally reinforced polymer composites, accompanied by extensive hackle formation, which is a common failure mode of epoxy exhibiting some ductility at the microscale.

One of the key findings of the microscopy study is that the addition of perforated release films to selected interfaces in unidirectional composite laminates alters the otherwise quasi-homogeneous architecture by creating a structured interlayer. The perforated film consistently remained on the central layer side of the interfaces as it moved together with this block during the mode II fracture test. The observed fracture surfaces were not smooth, exhibiting outstanding resin blocks at the perforation zones on the film side and featuring recesses on the corresponding no-film side of the delaminated interfaces. The patterned resin

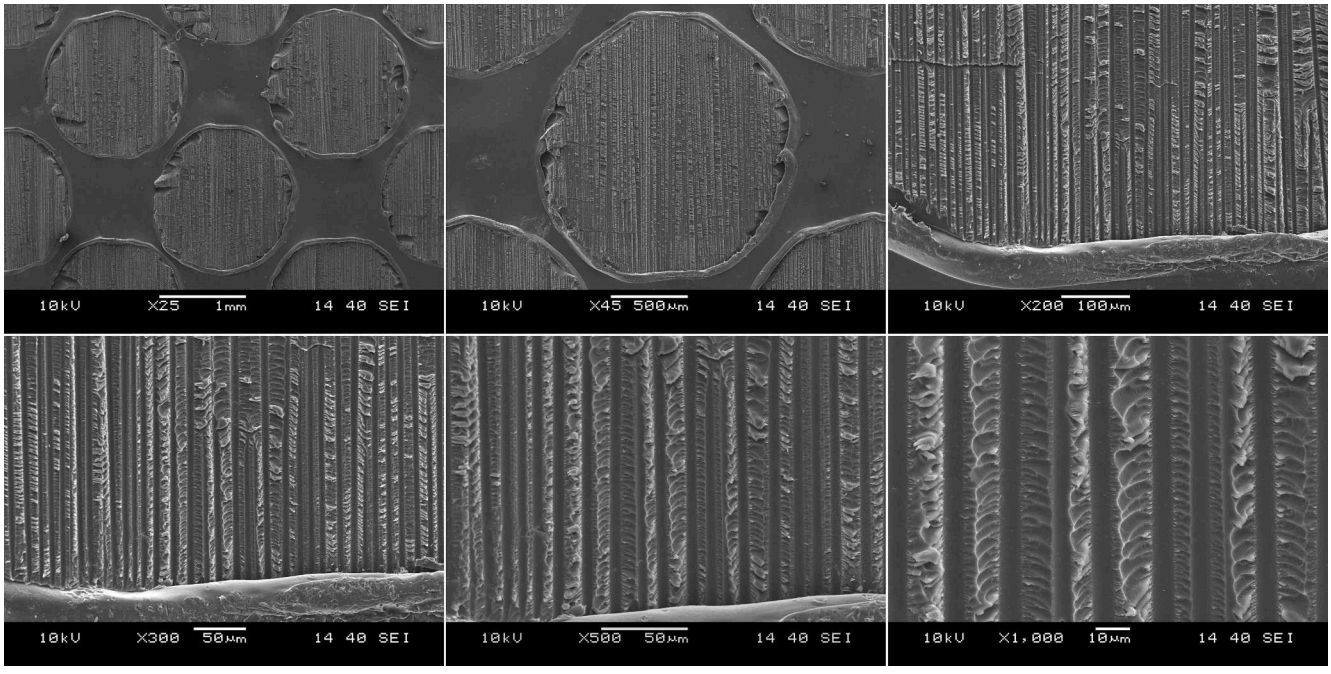

Fig. 12. Different magnification scanning electron micrographs taken from the film side of a delaminated interface of a D1.6mmICAR0.56 type sample with traces of debonded fibres on the surface.

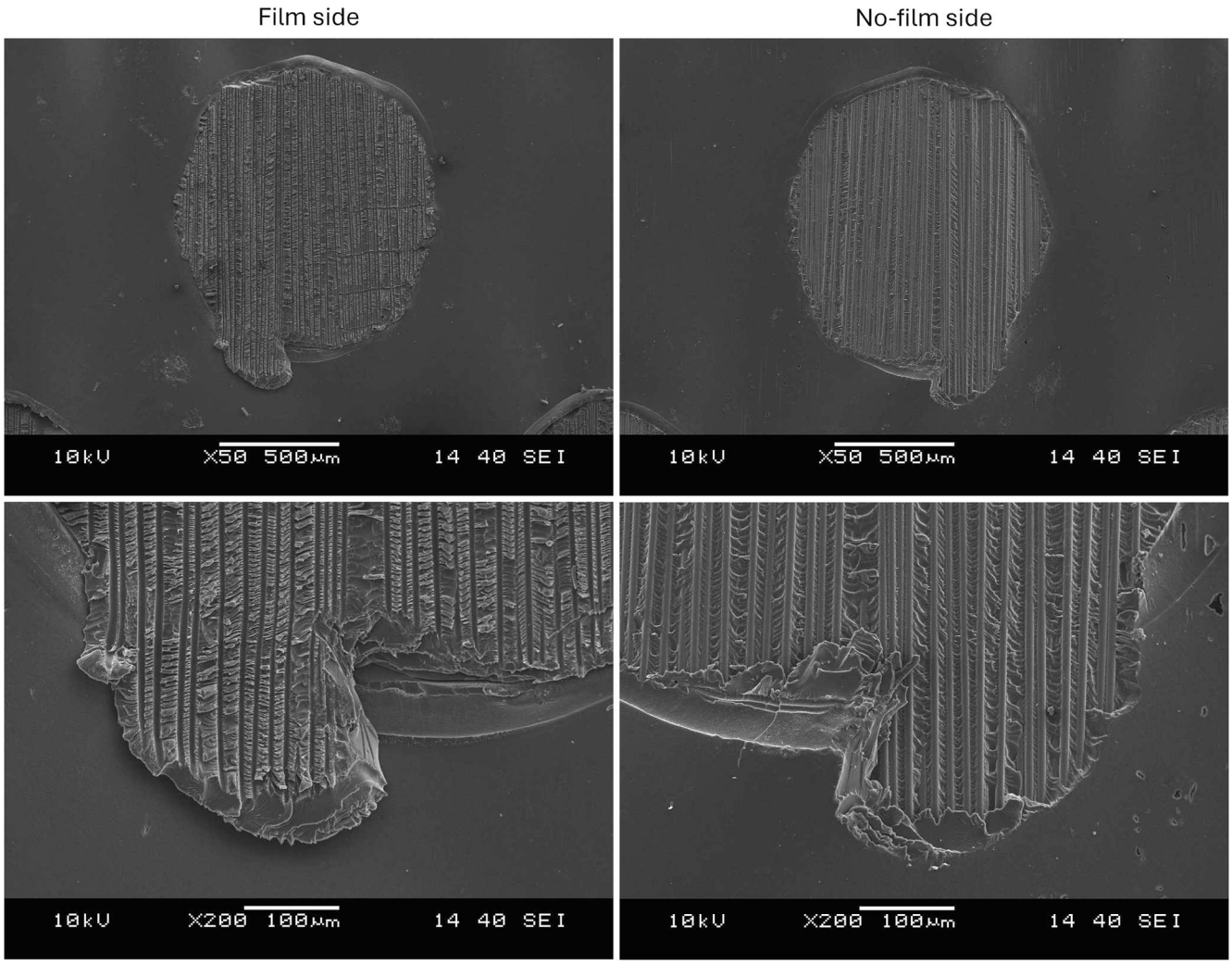

Fig. 13. Corresponding details of the two sides of a delaminated interface from a D1.1mmICAR0.25 type coupon (scanning electron micrographs).

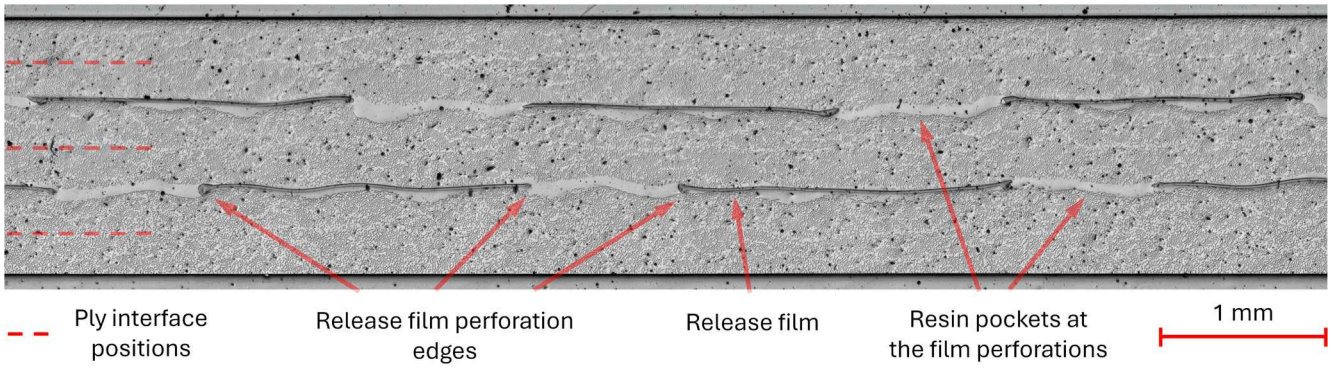

Fig. 14. Digital microscope image of the cross-section of a D1.1mmICAR0.25 type coupon before testing.

blocks, which joined the adjacent composite layers through the perforations of the release film, did not suffer shear fracture at the level of the release film but instead debonded from the densely packed fibres on the no-film side of the interface. The high slope of the trendlines in Fig. 10, and particularly the high G_{IIC} of the D1.6mmICAR0.56 type coupons (i.e. 10% higher than that of the baseline), is attributed to this unique fracture pattern. In cases of high ICAR perforation patterns, the resin blocks form a nearly continuous network with a notably long perimeter (see Fig. 12). Mode II fracture through this structured network of resin blocks is expected to absorb more energy than that of the much flatter interfaces of the baseline coupons. This additional fracture energy appears to counteract the fact that 44% of the full interface area, covered with release film, provides no or minimal adhesion.

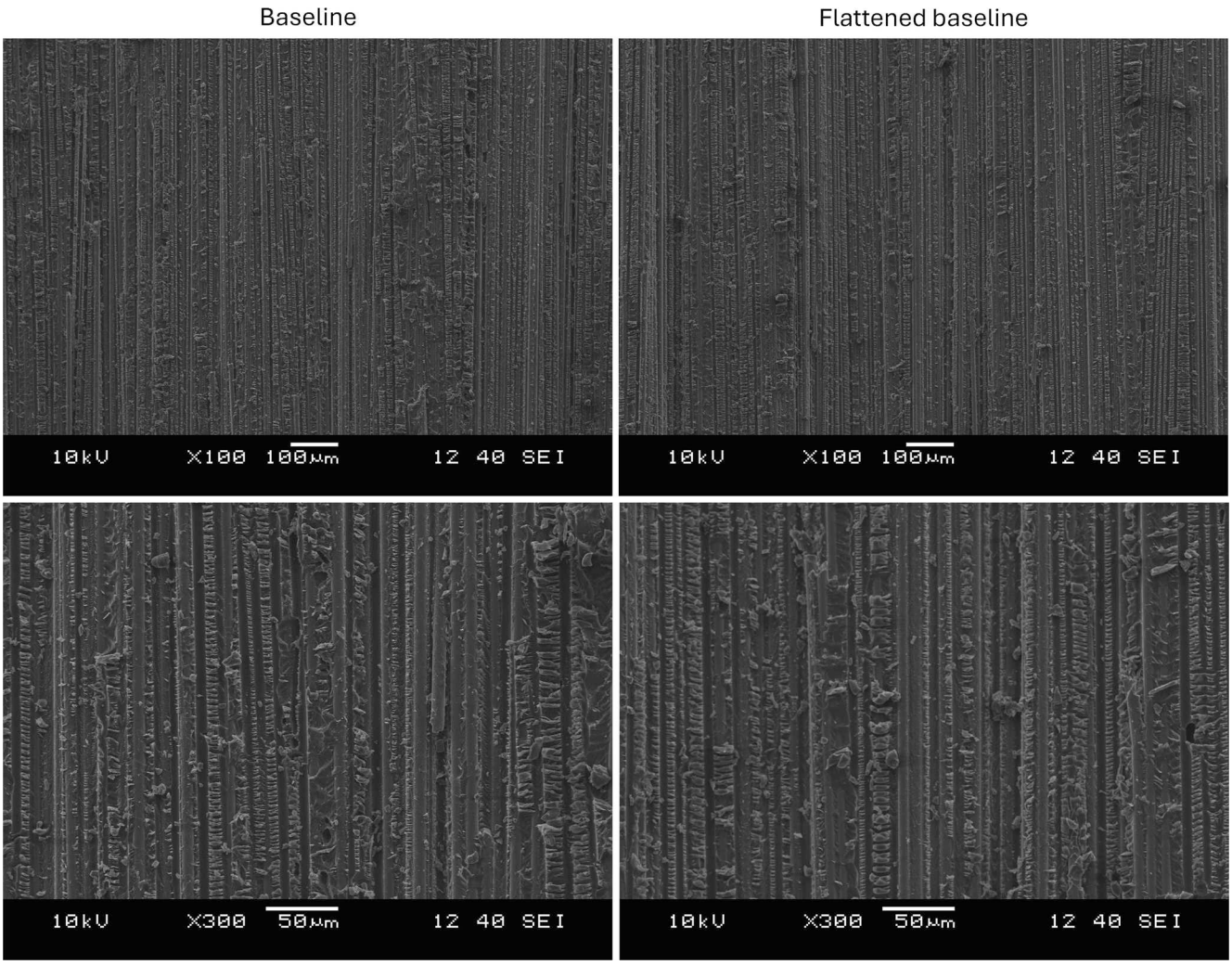

Fig. 15. Delaminated interfaces of a Baseline and a Flattened baseline sample (central layer side) with both debonded fibres and fibre traces.

8. Conclusions

The following conclusions were drawn from the study of different perforated release film layer interface modification configurations:

- Perforated release films with structured patterns were found to be suitable for controlling the mode II fracture toughness (G_{IIC}) of composite layer interfaces. Perforation patterns were systematically designed for geometrical characterisation and interface modification.
- Six laser-cut perforation patterns were analysed optically, and it was found that the actual perforation diameters were larger than the nominal values. The difference was similar across all configurations and did not depend on the nominal diameter, as it was due to the finite width of the cut line.
- The laser-cutting-induced increase in perforation diameters resulted in a difference between the nominal and actual interlaminar contact area ratios (ICAR), which is defined as the ratio of perforation areas to the total area of interest. The differences in the ICAR values showed a monotonic relationship with the total perforation length (needed to cover a given area with set perforation diameter and ICAR parameters).
- Unidirectional composite prismatic tensile test coupons with one-third of their plies cut in the central layer were found to be suitable for G_{IIC} assessment when the strain was measured over a section excluding the ply discontinuity zone.
- The G_{IIC} of the modified laminates exhibited a strong linear trend with increasing ICAR, enabling the precise design of perforation patterns to accurately control composite layer interface properties. The maximum reduction of G_{IIC} was up to 50% with the applied perforation patterns, but the test campaign results indicate that the full range may be covered if suitable perforation parameters are selected.
- Fractography of the delaminated interfaces revealed that the perforated release films created structured interlayers between the composite blocks, which failed in a unique way. Resin pockets at the perforations consistently remained bonded to the film side of the interfaces and debonded from the no-film side, leaving recesses.
- The effect of prepreg manufacturing induced transverse direction out-of-plane undulation on the G_{IIC} was analysed by flattening the ply blocks before lay-up. Baseline laminates with flattened interfaces (and no perforated release film) exhibited slightly lower G_{IIC} values than the pristine ones, despite only a small improvement in interface shape observed in cross-sectional micrographs.
- Interestingly, the perforation pattern with the highest ICAR (0.56) increased the G_{IIC} of the laminate by up to 10%. This indicates that the effect of structuring the interface was stronger than the separation effect of the remaining release film, covering 44% of the interface area. The high obtained G_{IIC} values are attributed to the additional energy required to fracture the structured interlayer of the modified coupons. Based on the presented findings, high ICAR

perforation patterns may be developed to achieve a limited yet well-controlled increase of G_{IIC} in composite laminates.

CRediT authorship contribution statement

Gergely Czél: Writing – review & editing, Writing – original draft, Visualization, Validation, Supervision, Resources, Methodology, Investigation, Funding acquisition, Formal analysis, Data curation, Conceptualization.

Declaration of competing interest

The author declare the following financial interests/personal relationships which may be considered as potential competing interests: Gergely Czel reports financial support was provided by National Research, Development and Innovation Office (NRDI, Hungary). Gergely Czel reports financial support was provided by Ministry of Culture and Innovation of Hungary. Gergely Czel reports financial support was provided by Hungarian Academy of Sciences. If there are other authors, they declare that they have no known competing financial interests or personal relationships that could have appeared to influence the work reported in this paper.

Acknowledgement

The research was supported by the National Research, Development and Innovation Office (NRDI, Hungary) through grant OTKA FK 131882. The author acknowledges the Ministry of Culture and Innovation of Hungary for support from the National Research, Development and Innovation Fund through grant no. NKKP ADVANCED 149578. The research was supported by the Ministry of Culture and Innovation of Hungary from the National Research, Development and Innovation Fund, under the TKP2021-NVA funding scheme through grant no. TKP-6-6/PALY-2021 and from the Complex Development funding scheme through grant no. 2022-2.1.1-NL-2022-00012 Creation of National Laboratories. The author is grateful for support through the János Bolyai Research Scholarship of the Hungarian Academy of Sciences. Special thanks to Ádám Stocker for his help with the experiments. The author acknowledges Aedus Space Ltd. for access to the laser cutting equipment.

Data availability

No data was used for the research described in the article.

References

[1] Wang J, Zhang X, Jiang L, Qiao J. Advances in toughened polymer materials by structured rubber particles. Prog Polym Sci 2019;98:101160. https://doi.org/10.1016/j.progpolymsci.2019.101160.
[2] Romhany G, Szebenyi G. Interlaminar crack propagation in MWCNT/fiber reinforced hybrid composites. Express Polym Lett 2009;3:145–51. https://doi.org/10.3144/expresspolymlett.2009.19.
[3] Romhány G, Szebényi G. Interlaminar fatigue crack growth behavior of MWCNT/carbon fiber reinforced hybrid composites monitored via newly developed acoustic emission method. Express Polym Lett 2012;6:572–80. https://doi.org/10.3144/expresspolymlett.2012.60.
[4] Gao C, Mu B, Cheng S, Xu Z. Effective interlaminar toughening of carbon fiber/epoxy composite laminates by extremely low loadings of monolayer graphene oxide. Polym Compos 2025;46(4):3321–31. https://doi.org/10.1002/pc.29173.
[5] Turcsan T, Meszaros L. Mechanical performance of hybrid thermoset composites: effects of matrix and reinforcement hybridization. Compos Sci Technol 2017;141:32–9. https://doi.org/10.1016/j.compscitech.2017.01.005.
[6] Sasidharan S, Anand A. Interleaving in composites for high-performance structural applications. Ind Eng Chem Res 2023;62(1):16–39. https://doi.org/10.1021/acs.iecr.2c03061.
[7] İnal O, Katnam KB, Potluri P, Soutis C. Progress in interlaminar toughening of aerospace polymer composites using particles and non-woven veils. The Aeronautical Journal 2022;126(1295):222–48. https://doi.org/10.1017/aer.2021.95.
[8] Marton GZ, Szebényi G. Influencing the damage process and failure behaviour of polymer composites – a short review. Express Polym Lett 2025;19(2):140–60. https://doi.org/10.3144/expresspolymlett.2025.11.
[9] Groleau MR, Shi YB, Yee AF, Bertram JL, Sue HJ, YangP C. Mode II fracture of composites interlayered with nylon particles. Compos Sci Technol 1996;56:1223–40. https://doi.org/10.1016/S0266-3538(96)00080-2.
[10] Marino SG, Czél G. Improving the performance of pseudo-ductile hybrid composites by film-interleaving. Compos A Appl Sci Manuf 2021;142:106233. https://doi.org/10.1016/j.compositesa.2020.106233.
[11] Marino SG, Czél G. Development and characterisation of reparable, film-interleaved, pseudo-ductile hybrid composites. Compos A Appl Sci Manuf 2023;169:107496. https://doi.org/10.1016/j.compositesa.2023.107496.
[12] Zhang T, Yasaee M. Influence of thermoplastic interleaves and its healing effect on the failure mechanisms of open-hole notched composite laminates. Compos Sci Technol 2022;227:109597. https://doi.org/10.1016/j.compscitech.2022.109597.
[13] Yasaee M, Bond IP, Trask RS, Greenhalgh ES. Mode I interfacial toughening through discontinuous interleaves for damage suppression and control. Compos A Appl Sci Manuf 2012;43(1):198–207. https://doi.org/10.1016/j.compositesa.2011.10.009.
[14] Yasaee M, Bond IP, Trask RS, Greenhalgh ES. Mode II interfacial toughening through discontinuous interleaves for damage suppression and control. Compos A Appl Sci Manuf 2012;43(1):121–8. https://doi.org/10.1016/j.compositesa.2011.09.026.
[15] Palazzetti R, Zucchelli A. Electrospun nanofibers as reinforcement for composite laminates materials – a review. Compos Struct 2017;182:711–27. https://doi.org/10.1016/j.compstruct.2017.09.021.
[16] Mahato B, Lomov SV, Shiverskii A, Owais M, Abaimov SG. A review of electrospun nanofiber interleaves for interlaminar toughening of composite laminates. Polymers 2023;15:1380. https://doi.org/10.3390/polym15061380.
[17] Marino SG, Kuželová KE, Czél G. Development of pseudo-ductile interlayer hybrid composites of standard thickness plies by interleaving polyamide 6 nanofibrous layers. Compos Sci Technol 2023;234. https://doi.org/10.1016/j.compscitech.2023.109924.
[18] Narongdej P, Denk J, Barjasteh E. Investigation of interlayer toughening of carbon fiber composites using non-woven polyamide veils under different curing pressures. J Compos Mater 2024;58(5):647–59. https://doi.org/10.1177/00219983241229245.
[19] Molnár K, Košťáková E, Mészáros L. The effect of needleless electrospun nanofibrous interleaves on mechanical properties of carbon fabrics/epoxy laminates. Express Polym Lett 2014;8:62–72. https://doi.org/10.3144/expresspolymlett.2014.8.
[20] Lomov SV, Molnár K. Compressibility of carbon fabrics with needleless electrospun PAN nanofibrous interleaves. Express Polym Lett 2016;10(1):25–35. https://doi.org/10.3144/expresspolymlett.2016.4.
[21] Vallack N, Sampson WW. Materials systems for interleave toughening in polymer composites. J Mater Sci 2022;57:6129–56. https://doi.org/10.1007/s10853-022-06988-1.
[22] Szebenyi G, Czigany T, Magyar B, Karger-Kocsis J. 3D printing-assisted interphase engineering of polymer composites: Concept and feasibility. Express Polymer Letters 2017;11(7):525–30. https://doi.org/10.3144/expresspolymlett.2017.50.
[23] Szebényi G, Magyar B, Czigany T. Achieving pseudo-ductile behavior of carbon fiber reinforced polymer composites via interfacial engineering. Adv Eng Mater 2021;23:2000822. https://doi.org/10.1002/adem.202000822.
[24] Magyar B, Czigany T, Szebényi G. Metal-alike polymer composites: the effect of inter-layer content on the pseudo-ductile behaviour of carbon fibre/epoxy resin materials. Compos Sci Technol 2021;215:109002. https://doi.org/10.1016/j.compscitech.2021.109002.
[25] Yao J, Niu K, Niu Y, Zhang T. Toughening efficiency and mechanism of carbon fibre epoxy matrix composites by PEK-C. Compos Struct 2019;229:111431. https://doi.org/10.1016/j.compstruct.2019.111431.
[26] Wagih A, Mahmoud HA, Tao R, Lubineau G. Towards tough thermoplastic adhesive tape by microstructuring the tape using tailored defects. Polymers 2023;15(2):259. https://doi.org/10.3390/polym15020259.
[27] Lubineau G, Alfano M, Tao R, Wagih A, Yudhanto A, Li X, et al. Harnessing extrinsic dissipation to enhance the toughness of composites and composite joints: a state-of-the-art review of recent advances. Adv Mater 2024;36:2407132. https://doi.org/10.1002/adma.202407132.
[28] Favre JP. Improving the fracture energy of carbon fibre-reinforced plastics by delamination promoters. J Mater Sci 1977;12:43–50. https://doi.org/10.1007/BF00738470.
[29] Li CJ, Felbeck DK. Increased fracture toughness of graphite-epoxy composites through intermittent interlaminar bonding. J Compos Mater 1980;14(3):245–59. https://doi.org/10.1177/002199838001400306.
[30] Jang BZ, Lieu YK, Chung WC, Hwang LR. Controlled energy dissipation in fibrous composites I controlled delamination. Polym Compos 1987;8:94–102. https://doi.org/10.1002/pc.750080205.
[31] Pegoretti A, Cristelli I, Migliaresi C. Experimental optimization of the impact energy absorption of epoxy–carbon laminates through controlled delamination. Compos Sci Technol 2008;68(13):2653–62. https://doi.org/10.1016/j.compscitech.2008.04.036.
[32] Kuhtz M, Hornig A, Gude M, Jäger H. A method to control delaminations in composites for adjusted energy dissipation characteristics. Mater Des 2017;123:103–11. https://doi.org/10.1016/j.matdes.2017.03.003.
[33] Kuhtz M, Hornig A, Richter J, Gude M. Increasing the structural energy dissipation of laminated fibre composite materials by delamination control. Mater Des 2018;156:93–102. https://doi.org/10.1016/j.matdes.2018.06.039.

[34] Prinz R., Gadke M.: Characterisation of interlaminar mode I and mode II fracture in CFRP laminates. In: Proceedings of the International Conference Spacecraft Structures and Mechanical Testing, 24-26 April 1991, Nordwijk, Netherlands. Pages 97-102. Link: https://apps.dtic.mil/sti/tr/pdf/ADA297417.pdf.
[35] Wisnom MR. On the increase in fracture energy with thickness in delamination of unidirectional glass fibre-epoxy with cut central plies. J Reinf Plast Compos 1992; 11:897–909. https://doi.org/10.1177/073168449201100802.
[36] ASTM D7905/D7905M: Standard Test Method for Determination of the Mode II Interlaminar Fracture Toughness of Unidirectional Fiber-Reinforced Polymer Matrix Composites, https://store.astm.org/d7905_d7905m-19e01.html.
[37] Scalici T, Pitarresi G, Catalanotti G, van der Meer FP, Valenza A. The transverse crack tension test revisited: an experimental and numerical study. Compos Struct 2016;158:144–59. https://doi.org/10.1016/j.compstruct.2016.09.033.
[38] Czél G, Jalalvand M, Wisnom MR, Canal LP, Gonzalez CD, LLorca J. Novel experimental procedure and determination of full displacement fields of delaminating composite layer interfaces for evaluation of the mode II cohesive law. Eng Fract Mech 2015;149:326–37. https://doi.org/10.1016/j.engfracmech.2015.06.060.
[39] Czél G, Bugár-Mészáros M, Wisnom MR. Combined effect of moisture and test temperature on the pseudo-ductility of thin-ply carbon/epoxy-glass/epoxy hybrid composites. Compos A Appl Sci Manuf 2023;165:107353/1-107353/11. https://doi.org/10.1016/j.compositesa.2022.107353.
[40] Czél G, Jalalvand M, Wisnom MR, Czigány T. Design and characterisation of high performance, pseudo-ductile all-carbon/epoxy unidirectional hybrid composites. Compos B Eng 2017;111:348–56. https://doi.org/10.1016/j.compositesb.2016.11.049.
[41] Czél G. Development of sandwich test coupons with continuous protective layers for accurate determination of the tensile failure strain of unidirectional carbon fibre reinforced composites. Compos A Appl Sci Manuf 2024;187:108440. https://doi.org/10.1016/j.compositesa.2024.108440.